Thermochimica Acta 510 (2010) 173–184

Contents lists available at ScienceDirect

Thermochimica Acta

journal homepage: www.elsevier.com/locate/tca

Crystallization behaviour of PEO with carbon-based nanonucleants for thermal energy storage

Kinga Pielichowska*, Krzysztof Pielichowski

Department of Chemistry and Technology of Polymers, Cracow University of Technology, ul. Warszawska 24, 31-155 Krakow, Poland

ARTICLE INFO

Article history:
Received 19 February 2010
Received in revised form 8 July 2010
Accepted 11 July 2010
Available online 16 July 2010

Keywords:
Phase change materials
Nanonucleants
Poly(ethylene oxide)
Crystallization

ABSTRACT

Carbon-based nanoadditives—carbon black, graphite, carbon fibres, single walls carbon nanotubes (SWCNTs) and fullerenes have been processed with poly(ethylene oxide) (PEO) using a melt-solidification method and characterized for thermal energy storage applications. Results of differential scanning calorimetry investigations for PEO and PEO/nanonucleant systems show that the temperature and heat of phase transition depend on the composition of the blends and kind of carbon additives. For the PEO/fullerene and PEO/SWCNTs blends, higher heats of melting in comparison to theoretical values have been observed, with the highest heat of melting for PEO/fullerenes (90/10, w/w) and PEO/SWCNTs (90/10, w/w). From isothermal kinetic analysis the Avrami exponent for PEO/SWCNTs was calculated as 1.81–2.19, while for PEO/fullerenes (90/10, w/w) its value was in the range of 1.41–2.02. Based on the Hoffman and Weeks theory it has been found that for crystallization of all samples under temperature conditions corresponding to the crystallization regime III, incorporation of SWCNTs and fullerenes lowers the activation energy of nucleation. A shift of absorption bands of C–O stretching vibrations in PEO/SWCNT and PEO/fullerene blends has been found as compared to PEO—the C_{60} and SWCNT molecules interact with PEO oxygen ethers and reduce the mobility of the polymer chains.

1. Introduction

Thermal energy storage materials are currently a subject of extensive research due to increasing awareness in energy management with the special attention focused on efficient use and conservation of the waste heat and solar energy in industry and buildings [1].

Fusion-solidification is the reversible phase-change process that is most frequently utilized or envisaged for practical applications. In that case thermal energy transfer occurs when a material changes from a solid to a liquid, or from a liquid to a solid ("phase change materials" (PCMs)). When PCM reaches the temperature at which it changes phase (melting point) it absorbs heat without getting hotter. When the ambient temperature in the space around the PCM material drops, the PCM solidifies, releasing its stored latent heat. PCM absorb and emit heat while maintaining a nearly constant temperature [2].

Materials to be used for phase change thermal energy storage must have a large latent heat and high thermal conductivity. They should have a melting temperature lying in the practical range of operation, melt congruently with minimum subcooling and be chemically stable, low in cost, non-toxic and non-corrosive. Materials that have been considered for this purpose are hydrated salts, paraffin waxes, fatty acids and eutectics of organic and non-organic compounds, as well as polymeric materials. Thermal and mechanical properties of the latter group of materials can be significantly improved by changing the crystallization behaviour through incorporation of nucleating agents. Among them, nanostructured particles with high surface area may effectively increase the crystallization rate of semicrystalline polymers [3].

For instance, Winey and co-workers [4] reported on single walled carbon nanotubes (SWCNTs) incorporation in polyethylene (PE). They found that nanotubes provide nucleation sites to polyethylene and accelerate the spherulite growth rate, while reducing the crystal dimensionality from spherulite to disk-shaped.

The crystallization behaviour of polypropylene (PP) in the presence of SWCNTs has also been reported [5–8]. Valentini et al. studied the effects of different SWCNTs' concentrations on the crystallization of isotactic PP. They found that the incorporation of SWCNTs accelerate the nucleation and crystal growth mechanisms of PP. These results find an explanation in terms of microstructural changes shown by Raman spectroscopy. The changes of the low frequency Raman bands demonstrate that, for the low nanotube

* Corresponding author. Current address: AGH University of Science and Technology, Faculty of Materials Science and Ceramics, Department of Biomaterials, Al. Mickiewicza 30, 30-059 Krakow, Poland. Fax: +48 12 6173371.
E-mail address: kingapie@agh.edu.pl (K. Pielichowska).

0040-6031/$ – see front matter © 2010 Elsevier B.V. All rights reserved.
doi:10.1016/j.tca.2010.07.012

concentration, the polymer is intercalated between nanotubes into bundles which can be disaggregated. On the other hand, when the nanotube concentration is high, the high quantity of nanotubes does not allow the intercalation of a high quantity of polymer between SWCNT' bundles [8].

In another study, Probst et al. investigated polyvinyl alcohol (PVA)/SWCNT nanocomposites [9]. It has been found that the carbon nanotubes' nucleation effect depended strongly on the amount of SWCNT—non-isothermal crystallization experiments showed that nanotubes initiate the nucleation process at weight fractions as low as 0.1%. Recently, Nogales et al. have found that SWCNTs did not influence the crystal structure of poly(butylene terephthalate) [10], but there was no information on the crystallization rate. Melt compounded SWCNTs have been shown to act as effective nucleating agents for poly(ethylene terephthalate) (PET) crystallization. The SWCNTs at a concentration as low as 300 ppm enhance the crystallization temperature during melt cooling by 10 °C, or reduced the melt's isothermal crystallization time by more than 50%. This, as well as the electrical conductivity threshold at 2 wt.% concentration, and the accompanying increase in tensile and storage moduli, indicate a good dispersion of the SWCNTs in the PET matrix. WAXD measurements proved oriented crystallization of PET during cooling from randomised melts containing oriented nanotubes, supporting the hypothesis that the SWCNTs induce crystallization of PET chains along the nanotubes [11].

More recently, poly(ethylene oxide) (PEO)/multi walls carbon nanotube (MWCNT) nanocomposites have been prepared by Jin et al. [12]. Authors found that crystallization behaviour of PEO in PEO/MWCNT nanocomposites was quite different from that in other polymer/CNT systems. The crystallization process was influenced by MWCNT, which led to a decrease in the spherical crystal growth and increase in spherical crystal size. Non-isothermal crystallization experiments showed that incorporation of MWCNTs and chemically modified MWCNTs reduced the crystallinity and restricted the spherical crystal growth of PEO. The nucleation sites' number decreased and spherical crystal size increased, compared to the neat PEO. Change of crystal structure from spherical to disk-like was evidenced by Avrami equation when MWCNT was added up to 1 wt.%. Moreover, FTIR revealed that the incorporation of MWCNTs has a significant influence on the C–O and C–H stretching vibrations of PEO, which could lead to a decrease in crystallinity and melting temperature of PEO in the blends.

In another work it was shown that the addition of the CNTs lowers the melting temperature of the nanocomposites. When the carbon nanotubes of 1.5 wt.% are embedded in the nanocomposites, the melting temperature was reduced by around 2 °C compared with that of the pure PEO. Authors suggested that the existence of the carbon nanotubes interferes with the formation of larger PEO crystallines and raises the total amount of the PEO crystalline in the nanocomposites [13].

Polymer/fullerene (C_{60}) complexes have been also obtained [14–16] in which the interaction between the two components is known to involve acceptor-like centers on the C_{60} molecules. Since poly(ethylene oxide) is a relatively non-polar linear polymer containing ether oxygens which are good electron-donors in forming hydrogen bonds and coordinating with other electron acceptors, molecular complexes can readily be formed with C_{60} which are stabilized by weak van der Waals interactions between host and guest molecules [17,18]. NMR experiments confirmed interactions between the ether oxygen of PEO and the π-system of C_{60} in the PEO/C_{60} molecular complex, which leads to a good dispersion of fullerene in polymer. The C_{60} molecules act as crosslinks in the PEO amorphous matrix and inhibit the mobility of polymer chains. On the other hand, the interactions between the polymer and fullerene also reduce the rapid isotropic rotation of C_{60} molecules to some extent [19].

PEO has very complex crystallization behaviour. Kovacs et al. [20] have presented study on the crystal growth rates and morphology of PEO fractions crystallized from the melt. Cheng et al. [21] performed detailed study on crystallization behaviour of PEO with different molecular weight and with polydyspersity 1.05. They described chain folding as well as isothermal thickening and thinning of PEO chains during crystallization [22]. Moreover, they discussed changes in crystal morphology during transitions between I/II and II/III regimes. More recently, Vyazovkin et al. found that poly(ethylene oxide) (PEO) crystallization appears to begin in regime II and then undergoes two consecutive changes that however cannot be clearly interpreted as regime III [23].

PEO systems as phase change materials for thermal energy storage have been investigated by us in a systematic way [2,24]. To improve their properties (to increase the nucleation rate and enthalpy of phase transition, as well as decrease supercooling) carbon nanonucleating agents were incorporated into PEO matrix. In this work we report on the phase behaviour of carbon/PEO blends (carbon black, graphite, carbon fibres, single walls carbon nanotubes and fullerenes) studied by DSC, MTDSC and FTIR techniques.

2. Experimental part

2.1. Materials

Carbon materials were as follows:

- Carbon black (N-220, CWB, Słupca, Poland).
- Graphite (Aldrich, Stainheim, Germany).
- Carbon fibres (Torayca®, Toray Industries, Inc., Decatur, AL, USA).
- Fullerenes (Fullerite®, mix of C_{60}/C_{70} at 9:1 ratio, Aldrich, Stainheim, Germany).
- Single walls carbon nanotubes (SWCNTs) (Faculty of Materials Engineering, Chalmers University of Technology, Sweden).

Poly(ethylene oxide) (PEO) was produced by Polysciences Co., Warrington, PA, USA. Molecular weight was determined by GPC performed at 40 °C on a Hewlett-Packard 1050 GPC System with a refractometric detector, using Shodex OH-Pac SB803 HQ 8 mm × 300 mm column from Showa Denko. Average molecular weights were determined as M_n = 9630 and M_w = 13060, M_w/M_n = 1.38. Degree of crystallinity (X_c) was calculated using DSC data as 0.92. The crystalline PEO phase presence was additionally confirmed by FTIR method (Bio-Rad FTS 165 spectrometer, KBr pellets, resolution 4 cm^{-1}) by the triplet peak of the C–O–C stretching vibration at 1153, 1106 and 1061 cm^{-1} with a maximum at 1106 cm^{-1}.

Blends were prepared by mixing weighed amounts of components in the melt, followed by subsequent solidification. The mixing process was performed by hand mixing until homogeneous blend was achieved. DSC profiles of the blends showed high reproducibility and repeatability, confirming thus the homogeneous distribution of fillers. Composition of blends of carbon/PEO blends was presented in Table 1.

2.2. Techniques

2.2.1. Differential scanning calorimetry (DSC) and modulated temperature differential scanning calorimetry (MTDSC)

For the dynamic DSC measurements a Netzsch DSC 200, operating in dynamic mode, was employed. Sample of ca. 5 mg weight was placed in sealed aluminium pan. The heating rate of 10 K/min and cooling rate of 10 K/min were applied; argon was used as an inert gas. Prior to use the calorimeter was calibrated with an indium

Table 1
Samples' description.

Blend	Ratio [w/w]
PEO/carbon black	95/5
	90/10
	85/15
	80/20
PEO/graphite	95/5
	90/10
	85/15
	80/20
PEO/carbon fibres	95/5
	90/10
	85/15
	80/20
PEO/fullerenes	95/5
	90/10
	85/15
	80/20
PEO/SWCNTs	95/5
	90/10
	85/15
	80/20

and mercury standards; an empty aluminium pan was used as reference. Liquid nitrogen was used as a cooling medium.

For the isothermal and MTDSC measurements a Mettler Toledo 822e was employed. Sample of ca. 5 mg weight was placed in sealed aluminium pan, and argon was used as an inert gas. Prior to use the calorimeter was calibrated with an indium and mercury standards; an empty aluminium pan was used as reference. Intracooler was used in the cooling mode. For isothermal measurements, samples first were heated up to the temperature of 80 °C, kept after melting for 10 min and then rapidly cooled at a cooling rate of 80 K/min to the crystallization temperature. For MTDSC measurements sinusoidal modulation was applied. Modulation parameters (period, amplitude and heating rate) are collected in Table 2.

2.2.2. Infrared spectroscopy (FTIR)

IR spectra of the samples (KBr pellets) were recorded on a Bio-Rad FTS 165 Fourier transform infrared (FTIR) spectrometer at a resolution of 2 cm^{-1}. The percentage of sample used to prepare the KBr pellets was approximately 2%

3. Results and discussion

Temperatures and heat of melting and crystallization for carbon/PEO systems are displayed in Table 3.

The additives used in the course of his work belong to two classes of fillers that are characterized by different dimensions of particles: nanoadditives (fullerenes and SWCNTs) and microadditives (carbon black, graphite and carbon fibres). After incorporation of nanoadditives into polymer matrix a large contact surface occurs

Table 2
MTDSC measurement conditions.

Amplitude [°]	Period [s]	Heating rate [K/min]
0.5	45	2
0.5	45	1
0.5	45	0.5
0.5	30	1
0.5	45	1
0.5	60	1
0.25	45	1
0.5	45	1
1	45	1

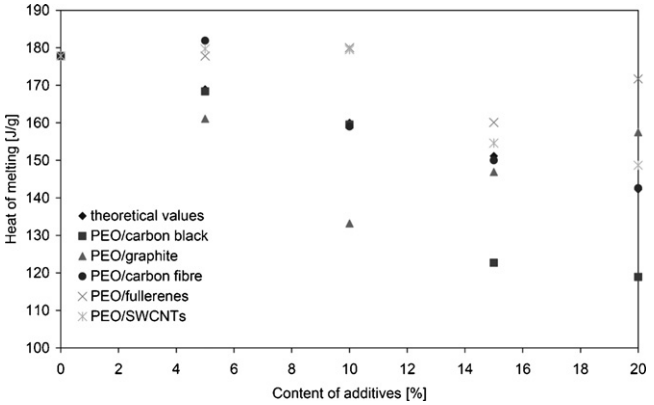

Fig. 1. Comparison of the theoretical and experimental values of the heats of melting for PEO/carbon additive blends.

(due to high specific area of nanoparticulates) and the amount of mutual interactions between the components is larger than in polymer/microadditive system. Consequently, nanoadditives do influence melting and crystallization processes more intensively than microfillers, as it can be seen in Fig. 1, where a synergistic effect of the heat of phase transition was observed for PEO/nanoadditive blends. This effect can be explained by efficient nucleation of the crystallization process by nanofillers and by strong interactions on molecular level.

For different polymer/additive systems various threshold values of the amount of additive that influence the phase change behaviour were found. By incorporation of too small amount of additive the crystallization process occurs at large superheating and the degree of crystallinity remains small, whereby by introducing of too much additive it may act as an impurity (inclusion) that hinders crystallization to proceed. The key issue is therefore a proper selection of the amount of additive—for instance, we have found that 5% is an optimum value for PEO/graphite and PEO/carbon black blends.

To compare the difference between experimental and theoretical values of the heat of phase transitions, theoretical values have been calculated according to the equation:

$$\Delta H_b = \Delta H_p x_p + \Delta H_a x_a \quad (1)$$

where ΔH_b is the heat of phase transition of the blend; ΔH_p is the heat of phase transition of the polymer; ΔH_a is the heat of phase transition of the additive; x_p and x_a are the weight fractions of polymer and additive, respectively. Results are presented in Fig. 1.

Results of DSC investigations of PEO and PEO/nanoadditive systems show that the temperature range and heat of phase transition depend on the composition of the blends and kind of carbon additives—Fig. 2.

The presence of the additive causes that PEO crystallization is hindered and depends on the ratio of the components. For PEO/carbon black blends with increase of carbon black content, a shift of the maximum of melting peak of PEO towards lower temperatures and a decrease of the heat of melting (in comparison to theoretical values), can be observed. For PEO/graphite composites no significant influence of graphite content on the melting temperature has been found, but the heat of melting depends on blends composition. For PEO/carbon fibre systems experimental values of heat of melting are in good agreement with theoretical ones. Also for the PEO/fullerene and PEO/SWCNT composites no significant influence of additive content on melting temperature has been observed. However, for all blends higher heat of melting in comparison to theoretical values has been observed—with the highest heat of melting for PEO/fullerene (90/10, w/w) and PEO/SWCNT (90/10, w/w) blends (even higher than for pure PEO). Moreover,

Table 3
Temperatures and heat of phase transition for melting and crystallization process for PEO/carbon additive blends.

Content of additives [wt.%]	Melting				Crystallization			
	T_{onset} [°C]	T_{max} [°C]	T_{end} [°C]	Heat of melting [J/g]	T_{onset} [°C]	T_{max} [°C]	T_{end} [°C]	Heat of crystallization [J/g]
PEO	57.8	63.7	67.9	177.8	36.1	31.1	26.6	170.0
Carbon black								
5	57.3	62.8	65.3	168.4	39.6	33.8	29.4	163.3
10	56.9	63.2	66.0	159.5	40.3	34.2	28.3	154.9
15	57.3	62.9	65.6	122.7	41.5	36.3	29.7	118.9
20	57.5	62.7	66.2	118.9	40.3	34.9	31.2	119.7
Graphite								
5	57.7	63.2	65.8	161.1	40.3	36.433.4	30.1	158.5
10	57.7	63.0	66.2	133.2	40.6	33.8	29.4	130.6
15	57.9	63.8	66.7	146.9	40.2	35.4	30.8	142.1
20	57.7	63.5	66.0	157.5	40.5	35.4	31.4	151.5
Carbon fibres								
5	56.8	63.4	67.4	181.9	41.6	35.6	30.5	177.5
10	57.4	63.6	66.5	159.0	42.0	33.9	29.5	155.3
15	58.1	63.6	66.7	150.0	42.7	37.5	34.0	146.2
20	56.8	63.5	66.7	142.6	42.9	38.434.3	30.6	140.6
Fullerenes								
5	57.8	63.7	67.9	177.8	36.1	31.1	26.6	170.0
10	57.9	63.5	66.7	180.0	44.0	36.7	32.9	175.4
15	57.7	63.2	66.3	160.1	44.0	38.4	34.7	157.5
20	58.4	63.8	67.3	171.7	45.5	40.4	35.8	170.8
SWCNTs								
5	58.5	64.1	66.7	179.7	41.6	34.1	30.6	178.1
10	57.6	63.4	66.2	179.5	41.4	33.4	29.8	176.1
15	57.5	62.5	66.3	154.6	41.2	33.2	29.7	150.0
20	57.4	62.3	68.4	148.7	40.0	35.0	29.8	147.3

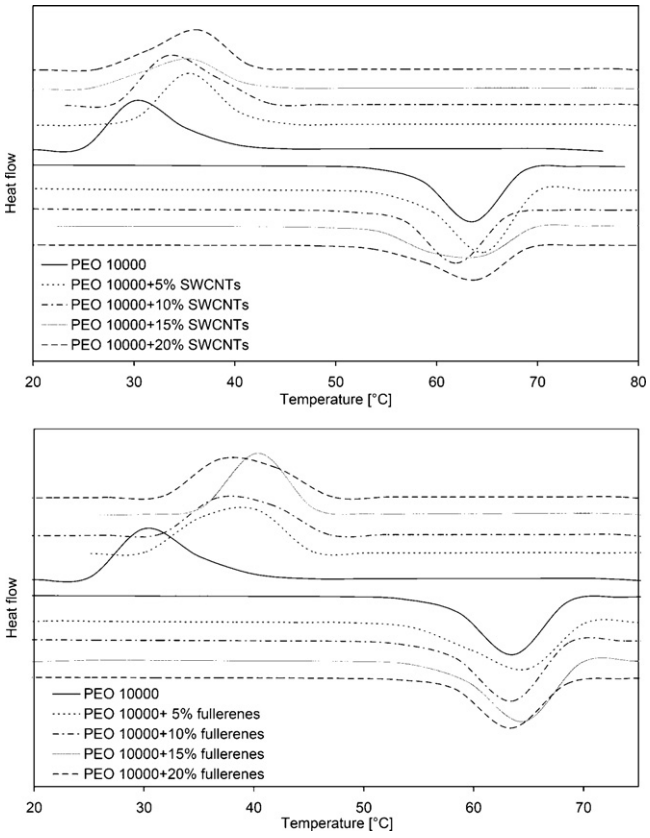

Fig. 2. DSC curves (in dynamic mode) for melting and crystallization processes of PEO/SWCNTs and PEO/fullerenes.

for all PEO nanonucleants systems a decrease of supercoooling has been revealed.

PEO/fullerenes (90/10) and PEO/SWCNTs (90/10) have been selected for further studies as representatives of PEO/fullerene and PEO/SWCNT blends, respectively, involving kinetic evaluation of isothermal crystallization process, MTDSC and FTIR investigations. The heat of phase transition has the highest value for PEO blends with 5 and 10 wt.% of SWCNTs, 10 wt.% of fullerenes and 5 wt.% of carbon fibres. For further studies we selected PEO blends containing the same amount (wt.%) of an additive to avoid differences arising from different additive content—PEO/fullerenes (10 wt.%) and PEO/SWCNTs (10 wt.%). For PEO blends with fullerenes and SWCNTs the heat of phase transition was higher than expected theoretical value (Fig. 1). For all other systems (except of PEO/carbon fibres 5 wt.%) it was equal or smaller. Besides, fullerenes cause a decrease of supercooling during PEO crystallization, which is an advantageous effect in terms of energy storage.

3.1. Kinetics of isothermal crystallization

The DSC profiles of PEO/fullerene (90/10, w/w) and PEO/SWCNT (90/10, w/w) blends' isothermal crystallization process are shown in Fig. 3.

From Fig. 3 it can be seen that isothermal DSC profiles of PEO/SWCNTs blends are more regular, as compared to pure PEO [25], but still several (2–4) maxima indicating an overlapping process can be observed—they origin from the crystallization of different PEO fractions (polydispersity degree of PEO was 1.38) at different temperatures. However, DSC profiles of PEO/fullerenes are smooth and regular with only one maximum, so all PEO fractions crystallize in the same time. These observations may suggest different nucleation and crystallization mechanisms as well as formation of different crystalline forms in PEO/SWCNTs and PEO/fullerenes systems.

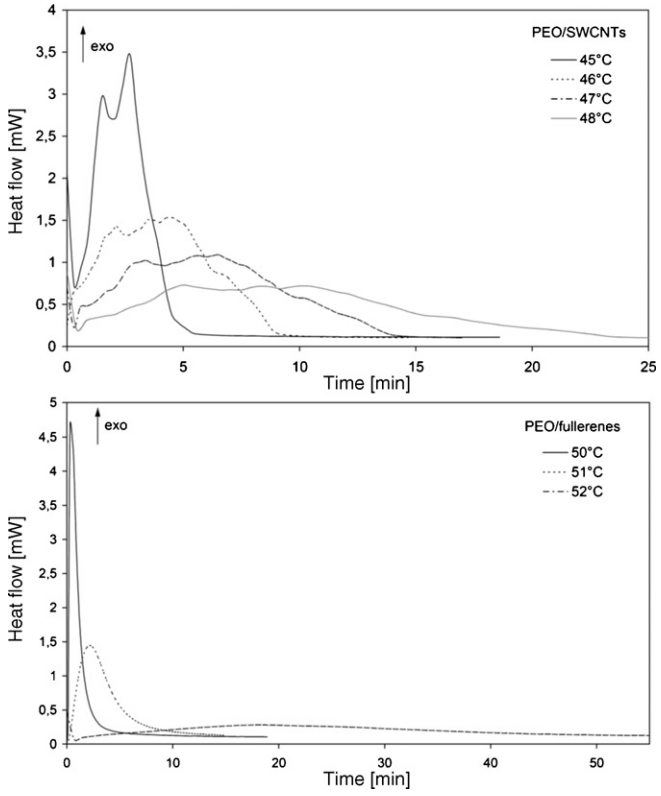

Fig. 3. DSC curves for isothermal crystallization process of PEO/10% SWCNTs and PEO/10% fullerenes.

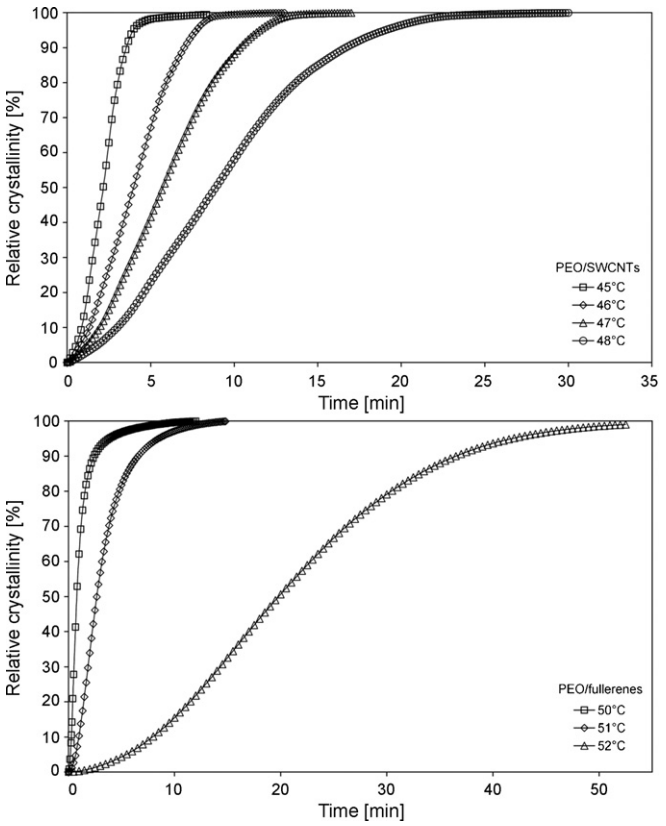

Fig. 4. Relative crystallinity vs crystallization time for PEO in PEO/10% SWCNT and PEO/10% fullerene systems crystallized at different temperatures.

As the crystallization temperature (T_c) increases, the exothermal peak is shifted to longer time, indicating that the T_c is an important factor influencing the crystallization time. The crystallization process is usually treated as a composition of two stages: the primary crystallization and the secondary crystallization. It is generally believed that the secondary crystallization is caused by the crystallization behaviour of microcrystallites at the interface between big spherulites in the later stage of crystallization process [26,27].

The relative crystallinity $X(t)$ of samples is obtained from the area of the exothermic peak in DSC isothermal crystallization analysis at a crystallization time t divided by the total area under the exothermic peak:

$$X_t = \frac{\int_0^t (dH/dt)dt}{\int_0^\infty (dH/dt)dt} \quad (2)$$

where dH/dt is rate of heat flow, the numerator is the heat generated at time t and the denominator is the total heat generated up to complete crystallization [28].

Fig. 4 shows the plots of relative crystallinity vs time for PEO/fullerenes (90/10, w/w) and PEO/SWCNTs (90/10, w/w) isothermally crystallized at different temperatures, in which the characteristic sigmoidal isotherms are shifted to right along the time axis with increasing T_c, and the whole crystallization time (t_c) is increasing with the crystallization temperature.

One can observe that the relative crystallinity increases quickly with an increase in crystallization time at the primary stage of crystallization, but this increase slows down at the later stage of crystallization. This phenomenon may result from the secondary crystallization of PEO [29].

Assuming that the relative crystallinity increases with an increase of the crystallization time t, Avrami equation (Eq. (3)) [30] can be used to analyse the isothermal crystallization process of PEO in PEO/fullerene (90/10, w/w) and PEO/SWCNT (90/10, w/w) blends, as follows:

$$X_t = 1 - \exp(-kt^n) \quad (3)$$

where X_t is the development of crystallinity at time t, k is the Avrami rate constant and n is the Avrami exponent. For the sake of convenience, Eq. (3) is usually rewritten in the double logarithmic form:

$$\log[-\ln(1 - X_t)] = \log\ k + n \log t \quad (4)$$

From the plot of $\log[-\ln(1 - X(t))]$ vs $\log t$, the n and $\log k$ values can be obtained from the slope and intercept, respectively—Fig. 5.

There is a series of straight lines almost parallel to each other at a primary stage of crystallization.

The crystallization half-time, $t_{1/2}$, is defined as the time at which the extent of crystallization is 50%, and is determined from the following relationship:

$$t_{1/2} = \left(\frac{\ln 2}{k}\right)^{1/n} \quad (5)$$

Usually, the rate of crystallization, G, is described as the reciprocal of $t_{1/2}$, that is

$G = \tau_{1/2} = 1/t_{1/2}$. The necessary time for maximum crystallization rate, t_{max} was calculated according to Eq. (5) [31].

$$t_{max} = \left(\frac{n-1}{nK}\right)^{1/n} \quad (6)$$

The values of T_c and Avrami parameters for investigated samples are listed in Table 4.

It can be found that both SWCNTs and fullerenes increase of the T_c of PEO by more than 5 K, which indicates an efficient nucleating effect induced by these two materials.

The Avrami exponent derived from isothermal crystallization reflects the nucleation mechanism and growth dimensions of the

Table 4
Isothermal crystallization kinetic parameters analysed by Avrami equation for PEO/10% SWCNT and PEO/10% fullerene blends.

Sample	T_c [°C]	n	k [min^{-n}]	t_{max} [min]	$t_{1/2}$ [min]	G [min^{-1}]
PEO 10000/10% SWCNTs	45	2.19	0.1391	1.86	2.08	0.4802
	46	1.84	0.0585	3.06	3.83	0.2608
	47	1.85	0.0290	4.45	5.56	0.1798
	48	1.81	0.0138	6.83	8.70	0.1149
PEO 10000/10% fullerenes	50	1.41	0.8230	0.48	0.88	1.1295
	51	1.58	0.1334	1.90	2.84	0.3523
	52	2.02	0.0016	17.05	19.94	0.0501

crystals. There are two kinds of nucleation—'homogeneous' and 'heterogeneous' one. Homogeneous nucleation is the process of birth of small regions of crystalline phase in the pure super-cooled melt, whereby heterogeneous nucleation is the process of birth of small crystalline regions on or near surfaces [32].

For instance, the confined crystallization of the block copolymer (a model system with controlled nano-sized morphology) is usually initiated by homogeneous nucleation and has a characteristic Avrami exponent $n \approx 1.0$, due to the much larger number of domains than that of heterogeneous nuclei [33–35].

On the other hand, most of the nucleation processes from the melt (that contains usually some heterogeneities or impurities) are of heterogeneous nature. Nucleating agents accelerate heterogeneous nucleation through the 'epitaxy' between nucleating agents and crystals or by suppression of mobility of macrochains [32].

The value of the Avrami exponent obtained from Table 4 for PEO/SWCNTs is 1.81–2.19.

Usually, these values can be interpreted as a mix of two mechanisms: (i) two dimensional crystal growth (for $2 < n < 3$, circular disk shape growth) with a linear growth rate and the crystal nucleating athermally, and (ii) one-dimensional needle-like crystal growth, nucleating thermally with diffusion-controlled rate (for $1 < n < 2$). The athermal nucleation implies that there is no contribution from nucleation rate to the activation energy [36,37]. But for PEO dilatometric measurements have given values of n approximately equal to 2 which would indicate crystal growth as discs or rods. However microscopic examinations clearly shows growth of spherulites [38]. Peculiarities of PEO which may complicate analysis of crystallization kinetics can be recognized—in part, the variation of the Avrami exponent, n, may be due to the very large size of spherulites which are formed so that crystallites initially forming as spheres may be constrained to become discs [39].

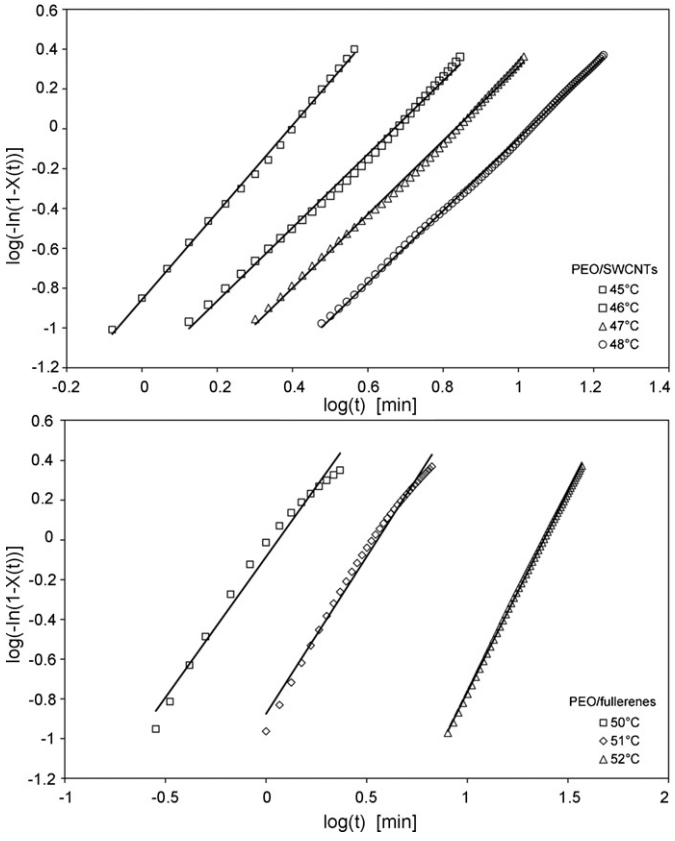

Fig. 5. Plots of $\lg\{-\ln[1-X(t)]\}$ vs $\lg t$ for isothermal crystallization of PEO in PEO/10% SWCNT and PEO/10% fullerene systems at different temperatures.

For PEO/fullerenes (90/10, w/w) values of the Avrami exponent are 1.41 and 2.02, respectively, which indicates the (ii) mechanism, and they stay in good agreement with literature data for PEO [38].

For the crystallization rate parameter (k) of PEO/fullerene (90/10, w/w) and PEO/SWCNT (90/10, w/w) blends it can be observed that the values of k are gradually decreasing with an increase of T_c. It confirms that in the isothermal crystallization process the higher is the T_c, the lower is the crystallization rate.

Turnbull and Fisher derived an equation for the rate of nucleation based on the small crystal model, and this equation is dominated by two opposing factors: the free energy of the nucleation barrier and the free energy of activation [40].

Effective activation energy (E) can be calculated from the Hoffman–Lauritzen theory [41,42] by using Eq. (7):

$$E = -R\frac{d\ln G}{dT^{-1}} = U * \frac{{T_c}^2}{(T_c - T_\infty)^2} + K_g R \frac{T_m^{0^2} - T_c^2 - T_m^0 T_c}{(T_m^0 - T_c)^2 T} \quad (7)$$

E depends on the parameters U^* and K_g that, respectively, represent the energy barriers of mass transport and nucleation. The effective activation energy decreases with increasing the temperature of crystallization. There are two major temperature regions for polymer crystallization: melt crystallization and cold crystallization. In the melt crystallization region, the measurements are performed by cooling a polymer from above T_m. The rate of crystallization decreases with increasing temperature giving rise to negative values of E. The growth rate is predominantly determined by the nucleation rate in that region. The cold crystallization region is typically accessed by heating glassy polymers. The respective values of E are positive as the rate of crystallization increases with increasing temperature. In this region the growth rate is mostly determined by mass transport. The two regions are separated by the temperature of the maximum growth rate, T_{max} at which the value of E approaches zero [43].

Hoffman and Lauritzen [44,45] utilized a lateral growth, surface-nucleation controlled process to describe the growth rates of polymer lamellar crystals. The Hoffman–Lauritzen theory suggests that the linear growth rate of a polymer crystal, G depends on temperature, T as follows:

$$G = G_0 \exp\left[\frac{-U*}{R(T_c - T_\infty)}\right] \exp\left[\frac{-K_g}{T_c(\Delta T)f}\right] \quad (8)$$

where G_0 is the preexponential factor, U^* is the activation energy of the molecular transfer through the melt–crystal interface, $\Delta T =$

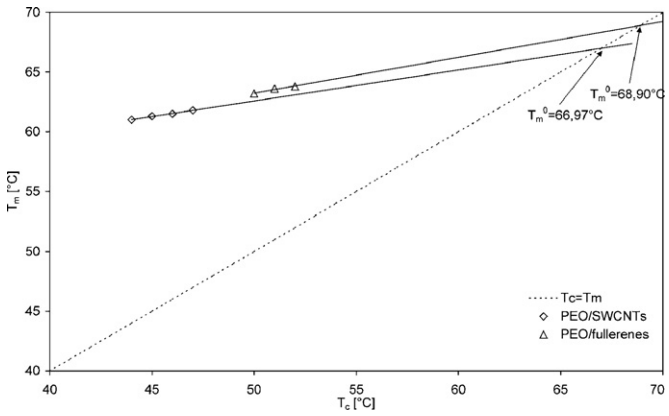

Fig. 6. Hoffman–Weeks plot for PEO/SWCNTs and PEO/fullerenes.

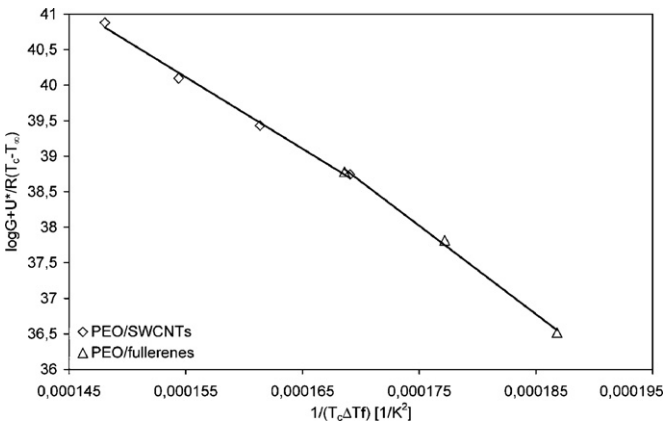

Fig. 7. Plot of $\log G + [U^*/R(T_c - T_\infty)]$ vs $1/(T_c \Delta T_f)$ for PEO/SWCNTs and PEO/fullerenes.

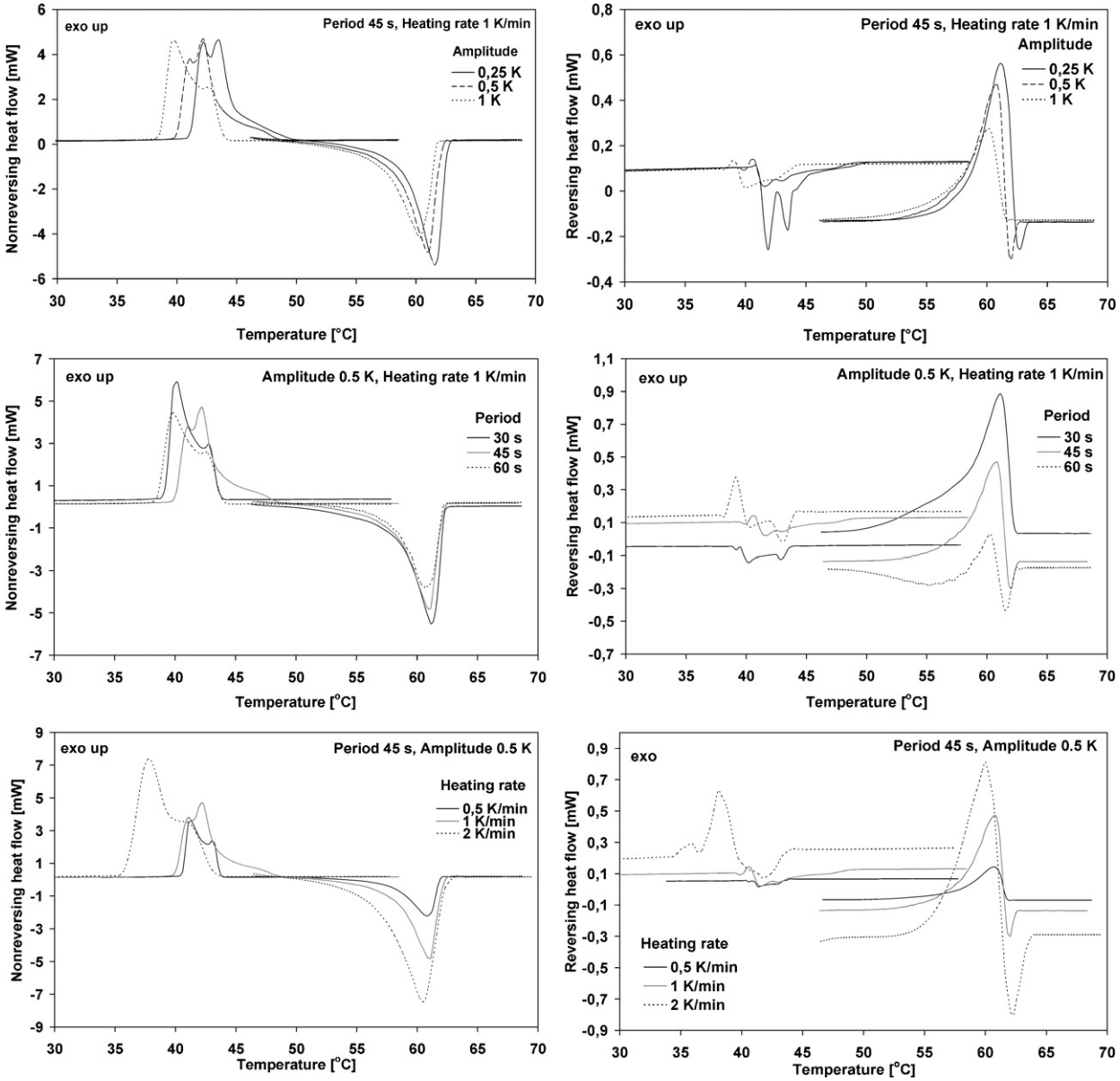

Fig. 8. MTDSC profiles for melting and crystallization processes of pure PEO.

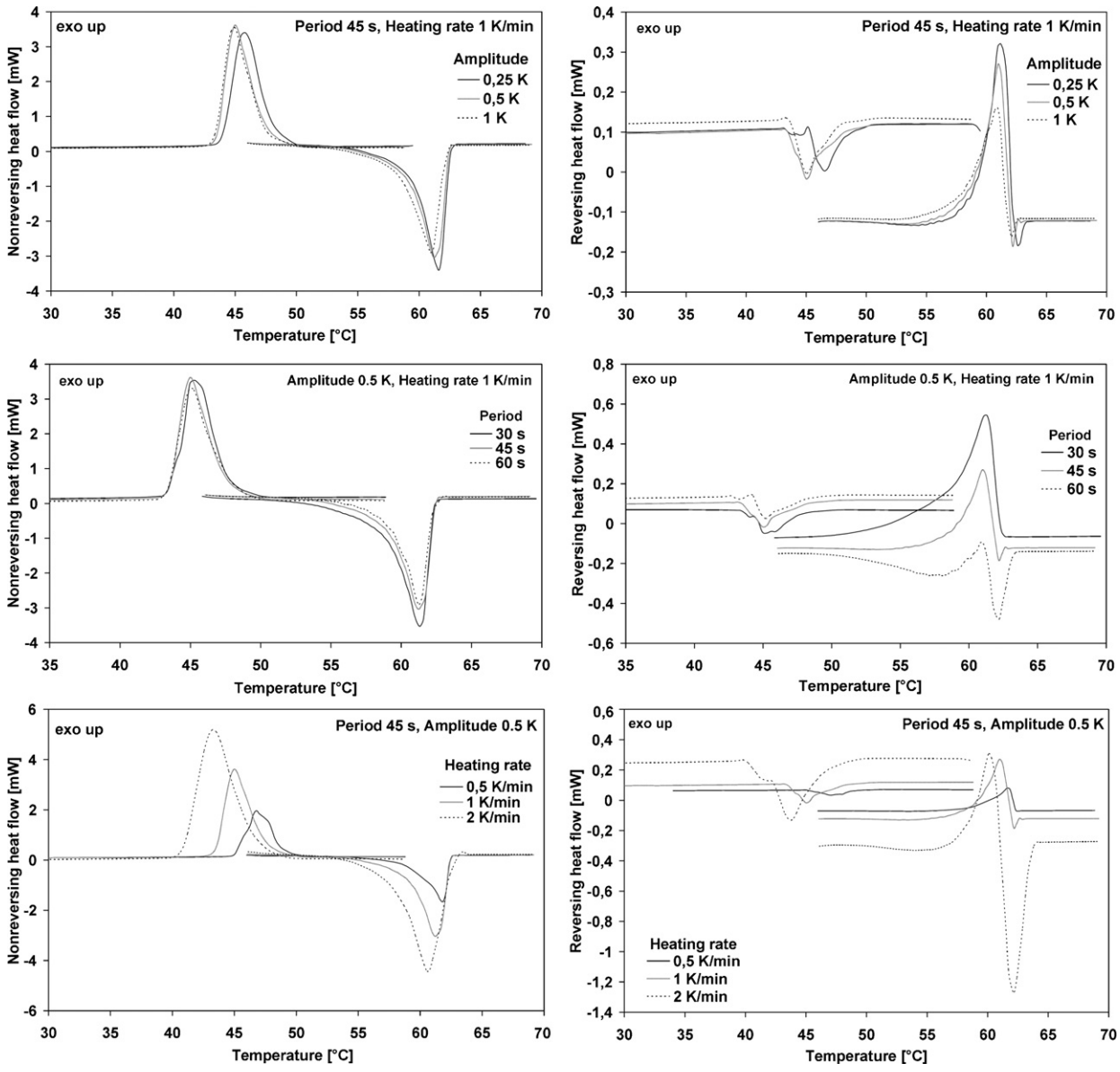

Fig. 9. MTDSC profiles for melting and crystallization processes of PEO/10% SWCNTs.

$T_m^0 - T_c$ is the undercooling, $f = 2T_c/(T_m^0 + T_c)$ is the correction factor, T_∞ is the hypothetical temperature at which viscous flow ceases (usually taken 30 K below the glass transition temperature, T_g).

The kinetic parameter K_g is the activation energy of nucleation for a crystal with a critical size and strongly depends on the degree of undercooling—it has the following form:

$$K_g = \frac{nb\sigma\sigma_e T_m^0}{\Delta h_f^0 k_B} \tag{9}$$

where b is the surface nucleus thickness, σ is the lateral surface free energy, σ_e is the fold surface free energy, T_m^0 is the equilibrium melting temperature, Δh_f^0 is the heat of fusion per

unit volume of crystal, k_B is the Boltzmann constant, and n takes the value 4 for crystallization regime I and III, and 2 for regime II.

From Eq. (8) in logarithmic form

$$\log\ G + \left[\frac{U*}{R(T_c - T_\infty)}\right] = \log G_0 - \frac{K_g}{T_c(\Delta T)f} \tag{10}$$

K_g can be determined from the linear plot of the left-hand side of this relationship plotted against $(T_c\Delta T_f)^{-1}$. The parameter U^* is either varied to determine the best linearity or, more frequently, is taken as the universal value 1.5 kcal/mol (i.e., 6.3 kJ/mol) [45]. Vyazovkin and Dranca [46] obtained parameters U^* and K_g from non-isothermal crystallization by applying an isoconversional method to DSC data. For PEO, Cheng et al. [21] used two values of U^*: 29.3 kJ/mol, quoted by Kovacs et al. [20], and 6.28 kJ/mol, the empirical 'universal' value suggested by Hoffman et al. [45]. Authors found that application of the empirical universal value of U^* (6.28 kJ/mol) obscured of regimes' transition. Hence, in our calculations we applied the value proposed by Kovacs (29.3 kJ/mol). Moreover, we used method proposed by Chan and Isaev [47], in which they replaced the growth rate with the reciprocal time to 50% of the relative crystallinity.

According to the theory derived by Hoffman and Weeks [48], the equilibrium melting temperature T_m^0 that is the melting temperature of infinitely extended crystals can be obtained by linear extrapolation of T_m vs T_c data to the line $T_m = T_c$. Fig. 6 shows the

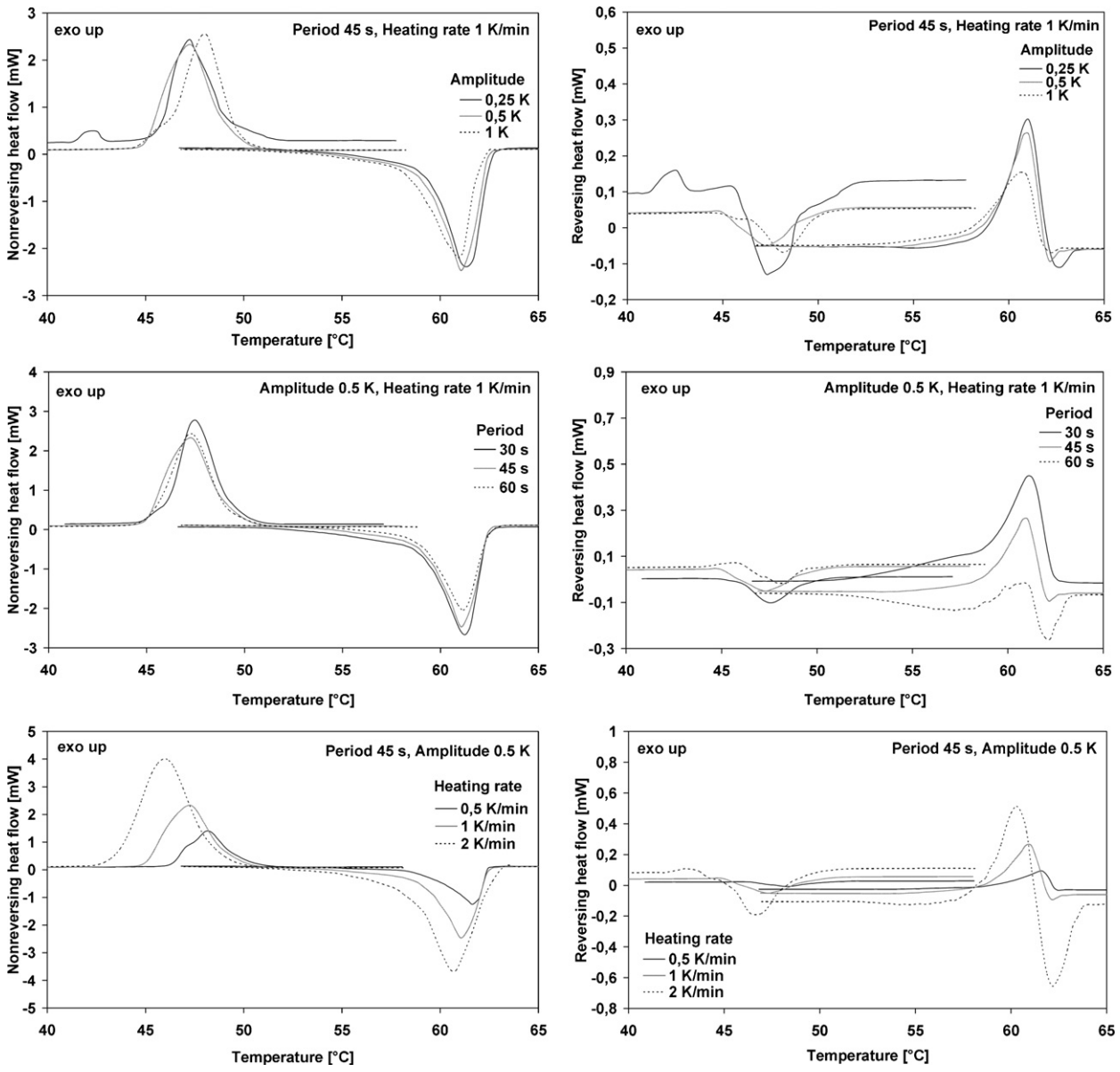

Fig. 10. MTDSC profiles for melting and crystallization processes of PEO/10% fullerenes.

plot of T_m vs T_c for PEO/SWCNTs and PEO/fullerenes. For pure PEO we assumed T_m^0 value of 342 K [49].

Plot of $\log G + [U^*/R(T_c - T_\infty)]$ vs $1/(T_c \Delta T_f)$ for PEO/SWCNTs and PEO/fullerenes is shown in Fig. 7

Cheng et al. [21] reported that at $\Delta T > 10\,^\circ$C crystallization occurs in regime II that is followed by a change to regime III at $\Delta T > 17.5\,^\circ$C. Assuming regime III crystallization ($n = 4$ in Eq. (9)) we estimated the value of $\sigma\sigma_e$. The value of Δh_f is 2.67×10^8 J m^{-3} [49], the b value is 4.65×10^{-10} m [50]. The obtained results are collected in Table 5.

One can draw a conclusion that for crystallization of all samples under temperature conditions corresponding to the crystallization regime III, incorporation of SWCNTs and fullerenes lowers the activation energy of nucleation.

Table 5
K_g and $\sigma\sigma_e$ parameters for PEO, PEO/SWCNTs and PEO/fullerenes.

Sample	$K_g \times 10^5$ [K^2]	T_m^0 [K]	U^* [kJ/mol]	$\sigma\sigma_e \times 10^4$ [J^2/m^4]
PEO	1.80	342	29.3	10.42
PEO/SWCNTs	1.00	340	29.3	23.31
PEO/fullerenes	1.25	342	29.3	28.96

3.2. MTDSC investigations

More information about the nature of thermal transitions in PEO/fullerene and PEO/SWCNT blends (in comparison to 'classical' DSC data) can be obtained if modulated temperature differential scanning calorimetry (MTDSC) is applied.

This technique offers extended temperature profile capabilities by e.g. sinusoidal wave superimposed to the normal linear temperature ramp. The modulated temperature and resultant modulated heat flow can be deconvoluted using a Fourier transform to give reversing and non-reversing components [51,52].

A DSC heating scan on a typical polymer contains many non-equilibrium effects, including a large amount of reversible melting due to metastability of crystal morphologies in most polymers [53]. The model of Zhou and Clough [54] qualitatively incorporates both dual crystal populations, early melting and recrystallization. In this model, early melting of secondary crystals contributes to the

low endotherm region, melting of primary crystals to the middle endotherm which is always present but not always distinguishable, and the final endotherm contains significant contributions from the recrystallized species formed during heating.

In recent experiments, Okazaki and Wunderlich found small amount of reversible melting and crystallization in PET by extending the time used in the quasi-isothermal mode because of "molecular nucleation" [55]. Molecular nucleation occurs when chains or chain segments melt near or on high-melting crystals, and then with negligible cooling, they can nucleate and recrystallize on these existing unmelted crystals. While this molecular nucleation process decreases due to annealing, it can occur continuously under "isothermal" conditions with an oscillation amplitude of 1 °C and a frequency of one reciprocal minute, and contributes to the so-called reversible signal in quasi-isothermal measurements. The "complete" melting of lamellae will contribute to non-reversing melting [56].

Elsewhere, in work of Cser et al. [57] the reversing heat flow has been measured and analysed as a function of time dependent parameters (heating/cooling rates, modulation period), and annealing experiments. They observed that the reversing heat flow measured by MTDSC and calculated using Fourier transform of the response of the equipment to the modulated temperature corresponds to the thermodynamically defined heat capacities. Moreover, there is a time dependent reversing part of the heat flow during the melting process. The longer time of modulation, the greater is the portion of reversing heat flow within the total heat flow. This dependence shows a relaxation type of transition during the melting process.

In this paper the influence of the three main measurement's parameters of MTDSC method: temperature amplitude (K), period (s) and heating rate (K/min) on the course of total, reversing and non-reversing components during the melting and crystallization of PEO, PEO/fullerene (90/10, w/w) and PEO/SWCNT (90/10, w/w) blends has been evaluated.

Results of the MTDSC measurements for PEO, PEO/SWCNT (90/10, w/w) and PEO/fullerene (90/10, w/w) systems at different conditions are shown in Figs. 8–10.

As it can be seen that for pure PEO, PEO/SWCNT (90/10, w/w) and PEO/fullerene (90/10, w/w) blends similar trends occurs for melting and crystallization process—higher amplitude causes a decrease in the total, non-reversing and reversing heat flow. By increasing the amplitude less privileged conditions for recrystallization (in the melting region) and partial melting (for melting and crystallization) are created and the total heat flow and non-reversing heat flow are therefore lower. Reversible melting is due to local equilibria of flexible chain segments within a metastable phase structure; poorer crystals show diffusional effects [52].

An increase of modulation period (decrease of frequency and average heating rate) increases the total heat flow for both melting and crystallization. By increasing the period, the equilibrium of reversible processes is shifted towards products and activation of rate-controlled processes takes place; chain nucleation is hampered and recrystallization proceed slower. This effect can be observed as a decrease of exothermic reversing signal and an increase of endothermic peak due to partial melting. Signal of the non-reversing component also decreases with an increase of period, because of smaller extent of recrystallization processes.

Heating rate plays an important role during the thermal analysis experiment—similarly, it influences considerably the shape of heat flow profiles under modulated conditions. If heating rate increases, reversing signal for the melting process becomes larger, both in exothermic and endothermic part due to induced recrystallization. Rate-controlled processes predominate in the total heat flow for measurements at higher heating rate; similarly, non-reversing heat flow also increases with an increase of the heating rate.

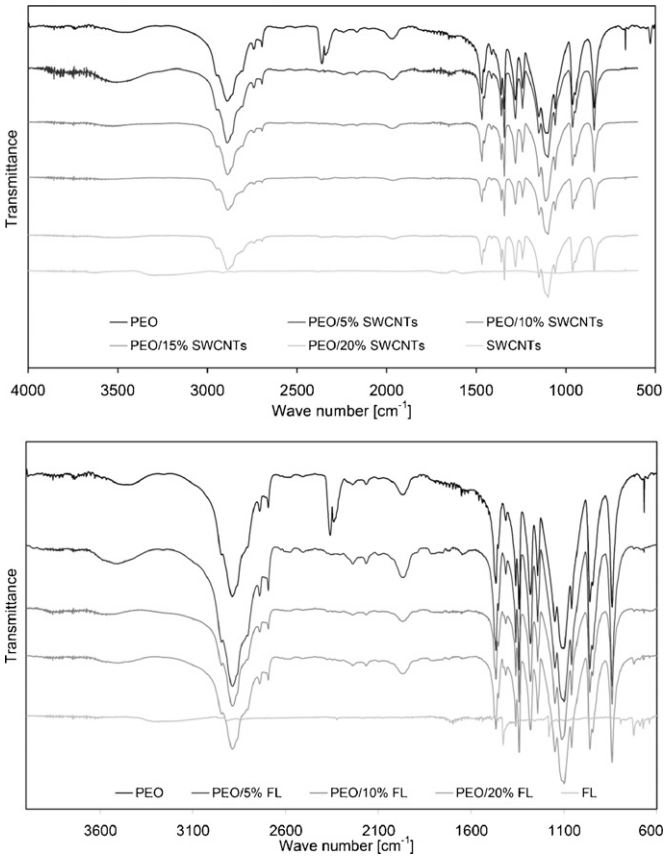

Fig. 11. FTIR spectra of PEO/SWCNT (a) and PEO/fullerene (b) blends.

More intense recrystallization leads to an increase of the total and non-reversing heat flow and affects partial melting (as evidenced by endothermic effect in reversing heat flow). This effect was observed for PEO/SWCNTs (90/10, w/w) and PEO/fullerenes (90/10, w/w) where the higher partial melting in the reversing heat flow profile has been observed. Moreover, even under different modulation conditions, only one maximum of peak originating from crystallization process for PEO/SWCNT and PEO/fullerene blends has been observed (for PEO a double-peak was found). It confirm our previous conventional DSC (dynamic and isothermal) results suggested different crystallization mechanism and formation of different crystalline forms in PEO blends in comparison to pure PEO.

NMR experiments indicate that there exist interactions between the ether oxygen of PEO and the π-system of C_{60} in the PEO/C_{60} molecular complex [19]. This kind of interaction should change the force constant of C–O bond that can be measured by FTIR method.

FTIR spectra for PEO 10000, PEO/SWCNTs (90/10, w/w) and PEO/fullerenes (90/10, w/w) are presented in Fig. 11 and described in Table 6.

Results of FTIR analysis of PEO in solid state stay in good agreement with NMR data—a shift of absorption bands from stretching vibrations of C–O groups in PEO/SWCNTs and PEO/fullerenes can be observed with the strongest shift in case of PEO/SWCNT (90/10, w/w) (1114 cm^{-1}) and PEO/fullerene (90/10, w/w) (1113 cm^{-1}) systems in comparison to pure PEO (1105 cm^{-1}).

Similar effect was observed in the work of Jin et al. [12], who investigated crystallization behaviour of PEO/MWCNTs and PEO/chemically modified MWCNTs. They found that MWCNTs show significant influence on the C–O and C–H stretching vibrations of PEO; FTIR analysis confirmed that C–O stretching vibration

Table 6
Description of characteristic bands for PEO 10000, PEO/SWCNTs (90/10, w/w) and PEO/fullerenes (90/10, w/w).

Wave number [cm^{-1}]							Assignment
PEO	PEO/5% SWCNTs	PEO/10% SWCNTs	PEO/20% SWCNTs	PEO/5% fullerenes	PEO/10% fullerenes	PEO/20% fullerenes	
3200–3600		3534	3520	3513	3567	3503	OH stretching, intramolecular hydrogen bonds
2883	2888	2886	2886	2889	2889	2889	CH_2 symmetric stretching
2861							CH_2 symmetric stretching
1466	1468	1467	1467	1468	1468	1468	CH_2 scissoring
1454	1455	1456	1455	1455	1455	1455	CH_2 scissoring
1412	1413	1413	1413	1413	1413	1413	CH_2 wagging
1361	1360	1360	1360	1360	1360	1360	CH_2 wagging
1340	1342	1343	1342	1342	1343	1342	CH_2 wagging
1280	1281	1281	1281	1281	1281	1281	CH_2 twisting
1241	1242	1242	1242	1242	1242	1242	CH_2 twisting
1148	1150	1150	1150	1150	1150	1150	C–O stretching, CH_2 rocking
1105	1100	1114	1100	1100	1113	1100	C–O stretching
1059	1060	1060	1060	1060	1060	1060	C–O, C–C stretching, CH_2 rocking
945	947	947	947	947	947	946	CH_2 rocking (gauche), C–C stretching,
842	842	842	842	842	842	842	C–O, C–C stretching, CH_2 rocking

of nanocomposites containing MWCNT–COOH and MWCNT–OH has shifted towards higher frequency of 1116 cm^{-1} compared to the pure PEO (1109 cm^{-1}).

The FTIR help to explain DSC data—the C_{60} molecules act as crosslinks in the PEO amorphous matrix and inhibit through molecular interactions the mobility of polymer chains. Similar effects for SWCNTs (containing six-unit structures with acceptor-like centers) has been also observed.

4. Conclusions

Results of DSC investigations for PEO and carbon/PEO systems show that the temperature range and heat of phase transition depend on the composition of the blends and kind of carbon additives. For the PEO/fullerene and PEO/SWCNT systems no significant influence of additive content on melting temperature of PEO/nanonucleant systems has been observed. However, for all systems higher heat of melting in comparison to theoretical values has been observed—with the highest heat of melting for PEO/fullerene (90/10, w/w) and PEO/SWCNT (90/10, w/w) systems. The values of the Avrami exponent for PEO/SWCNTs is 1.88–2.20, whereby for PEO/fullerenes (90/10, w/w) crystallized at temperatures 50 and 51 °C the values of the Avrami exponent are 1.69 and 1.82, respectively. For PEO/SWCNTs Avrami exponent values can be interpreted as a mix of two mechanisms: (i) two dimensional crystal growth (for $2 < n < 3$, circular disk shape growth) with a linear growth rate and the crystal nucleating athermally, and (ii) one-dimensional needle-like crystal growth, nucleating thermally with diffusion-controlled rate (for $1 < n < 2$). Crystallization of PEO/fullerenes (90/10, w/w) follows (ii) mechanism. On the basis of the Hoffman and Weeks theory it has been found that for crystallization of all samples under temperature conditions corresponding to the crystallization regime III, incorporation of SWCNTs and fullerenes lowers the activation energy of nucleation. MTDSC data confirm previous conventional DSC results (dynamic and isothermal), suggesting different crystallization mechanisms of PEO blends in comparison to pure PEO. Shift of absorption bands from stretching vibrations of C–O groups in PEO/SWCNT and PEO/fullerene systems has been observed in comparison to pure PEO with the strongest shift for PEO/SWCNT (90/10, w/w) and PEO/fullerene (90/10, w/w) systems—the C_{60} and SWCNTs molecules due to interactions with oxygen ether act as crosslinks in the PEO amorphous matrix and inhibit the molecular mobility of polymer chains.

Acknowledgement

Authors are grateful to prof. Rodney Rychwalski from Chalmers University of Technology for kind supply of SWCNTs.

References

[1] M.M. Farid, A.M. Khudhair, S.A.K. Razack, S. Al-Hallaj, A review on phase change energy storage: materials and applications, Energ. Convers. Manage. 45 (2004) 1597–1615.
[2] K. Pielichowski, K. Flejtuch, Differential scanning calorimetry study of blends of poly(ethylene glycol) with selected fatty acids, Macromol. Mater. Eng. 288 (2003) 259–264.
[3] G.Z. Papageorgiou, D.S. Achilias, D.N. Bikiaris, G.P. Karayannidis, Crystallization kinetics and nucleation activity of filler in polypropylene/surface-treated SiO_2 nanocomposites, Thermochim. Acta 427 (2005) 117–128.
[4] R. Haggenmueller, J.E. Ficher, K.I. Winey, Single wall carbon nanotube/polyethylene nanocomposites: nucleating and templating polyethylene crystallites, Macromolecules 39 (2006) 2964–2971.
[5] B.P. Grady, F. Pompeo, R.L. Shambaugh, D. Resasco, Nucleation of polypropylene crystallization by single-walled carbon nanotubes, J. Phys. Chem. B 106 (2002) 5852–5858.
[6] L. Valentini, J. Biagiotti, J.M. Kenny, S. Santucci, Effects of single-walled carbon nanotubes on the crystallization behavior of polypropylene, J. Appl. Polym. Sci. 87 (2003) 708–713.
[7] A.R. Bhattacharyya, T.V. Sreekumar, T. Liu, S. Kumar, L.M. Ericson, R.H. Hauge, R.E. Smalley, Crystallization and orientation studies in polypropylene/single wall carbon nanotube composite, Polymer 44 (2003) 373–377.
[8] L. Valentini, J. Biagiotti, J.M. Kenny, S. Santucci, Morphological characterization of single-walled carbon nanotubes-PP composites, Compos. Sci. Technol. 63 (2003) 1149–1153.
[9] O. Probst, E.M. Moore, D.E. Resasco, B.P. Grady, Nucleation of polyvinyl alcohol crystallization by single-walled carbon nanotubes, Polymer 45 (2004) 4437–4443.
[10] A. Nogales, G. Broza, Z. Rosłaniec, K. Schulte, I. Sics, B.S. Hsiao, Low percolation threshold in nanocomposites based on oxidized single wall carbon nanotubes and poly(butylene terephthalate), Macromolecules 37 (2004) 7669–7672.
[11] K. Anoop Anand, U.S. Agarwal, R. Joseph, Carbon nanotubes induced crystallization of poly(ethylene terephthalate), Polymer 47 (2006) 3976–3980.
[12] J. Jin, M. Song, F. Pan, A DSC study of effect of carbon nanotubes on crystallisation behaviour of poly(ethylene oxide), Thermochim. Acta 456 (2007) 25–31.
[13] Y.S. Song, Rheological characterization of carbon nanotubes/poly(ethylene oxide) composites, Rheol. Acta 46 (2006) 231–238.
[14] G. Yu, J. Gao, J.C. Hummelen, F. Wudl, A.J. Heeger, Polymer photovoltaic cells: enhanced efficiencies via a network of internal donor–acceptor heterojunctions, Science 270 (1995) 1789–1791.

[15] M. Cha, N.S. Sariciftci, A.J. Heeger, J.C. Hummelen, F. Wudl, Enhanced nonlinear absorption and optical limiting in semiconducting polymer/methanofullerene charge transfer films, Appl. Phys. Lett. 67 (1995) 3850–3852.
[16] J. Bruening, B. Friedman, Photoinduced charge transfer in conducting polymer C_{60} composites, J. Chem. Phys. 106 (1997) 9634–9638.
[17] J.J. Point, C. Coutelier, Linear high polymers as host in intercalates. Introduction and example, J. Polym. Sci. Polym. Phys. Ed. 23 (1985) 231–239.
[18] J.J. Point, B. Jasse, M. Dosiere, Intercalates with linear polymer hosts. Part 2. Fourier transform infrared study of poly(ethylene oxide)-p-disubstituted benzene intercalates, J. Phys. Chem. 90 (1986) 3273–3277.
[19] M. Li, Q. Chen, Interactions between fullerene(C_{60}) and poly(ethylene oxide) in their complexes as revealed by high-resolution solid-state ^{13}C NMR spectroscopy, Polymer 44 (2003) 2793–2798.
[20] A.J. Kovács, C. Straupe, A. Gonthier, Isothermal growth, thickening, and melting of poly(ethylene oxide) single crystals in the bulk. II, J. Polym. Sci., Polym. Symp. 59 (1977) 31–54.
[21] S.Z.D. Cheng, J. Chen, J.J. Janimak, Crystal growth of intermediate-molecular-mass poly(ethylene oxide) fractions from the melt, Polymer 31 (1990) 1018–1024.
[22] S.Z.D. Cheng, J. Chen, Nonintegral and integral folding crystal growth in low-molecular mass poly(ethylene oxide) fractions. III. Linear Crystal growth rates and crystal morphology, J. Polym. Sci. Part B: Polym. Phys. 29 (1991) 311–327.
[23] S. Vyazovkin, J. Stone, N. Sbirrazzuoli, Hoffman–Lauritzen parameters for non-isothermal crystallization of poly(ethylene terephthalate) and poly(ethylene oxide) melts, J. Therm. Anal. Calorim. 80 (2005) 177–180.
[24] K. Pielichowska, S. Głowinkowski, J. Lekki, D. Binias, K. Pielichowski, J. Jenczyk, PEO/carboxylic acid blends for thermal energy storage materials. Structural/morphological features and hydrogen interactions, Eur. Polym. J. 44 (2008) 3344–3360.
[25] K. Pielichowska, K. Pielichowski, Kinetics of isothermal and non-isothermal crystallization of poly(ethylene oxide) (PEO) in PEO/fatty acid blends, J. Macromol. Sci. Part B: Phys., submitted for publication.
[26] Y. Long, R.A. Shanks, Z.H. Stachurski, Kinetics of polymer crystallisation, Prog. Polym. Sci. 20 (1995) 651–701.
[27] M. Run, Ch. Yao, Y. Wang, Morphology, isothermal and non-isothermal crystallization kinetics of poly(methylene terephthalate), Eur. Polym. J. 42 (2006) 655–662.
[28] X. He, D. Xie, D. Yang, Isothermal crystallization kinetics of poly(trimethylene terephthalate) under the influence of self-seeding nucleation, Front. Chem. China 2 (2007) 222–226.
[29] J.N. Hay, P.J. Mills, The use of differential scanning calorimetry to study polymer crystallization kinetics, Polymer 23 (1982) 1380–1384.
[30] M. Avrami, Granulation, phase change, and microstructure kinetics of phase change. III, J. Chem. Phys. 9 (1941) 177–184.
[31] C.C. Lin, The rate of crystallization of poly(ethylene terephthalate) by differential scanning calorimetry, Polym. Eng. Sci. 23 (1983) 113–116.
[32] K. Okada, K. Watanabe, T. Urushihara, A. Toda, M. Hikosaka, Role of epitaxy of nucleating agent (NA) in nucleation mechanism of polymers, Polymer 48 (2007) 401–408.
[33] J.-T. Xu, J.P.A. Fairclough, S.-M. Mai, Ch. Chaibundit, Isothermal crystallization kinetics and melting behavior of poly(oxyethylene)-b-poly(oxybutylene)/poly(oxybutylene) blends, Macromolecules 35 (2002) 6937–6945.
[34] L. Zhu, B.R. Mimnaugh, Q. Ge, R.P. Quirk, S.Z.D. Cheng, E.L. Thomas, B. Lotz, B.S. Hsiao, F. Yeh, L.Z. Liu, Hard and soft confinement effects on polymer crystallization in microphase separated cylinder-forming PEO-b-PS/PS blends, Polymer 42 (2001) 9121–9131.
[35] Y.L. Loo, R.A. Register, A.J. Ryan, Polymer crystallization in 25-nm spheres, Phys. Rev. Lett. 84 (2000) 4120–4123.
[36] J. Li, Ch. Zhou, G. Wang, Y. Tao, Q. Liu, Y. Liet, Isothermal and nonisothermal crystallization kinetics of elastomeric polypropylene, Polym. Test. 21 (2002) 583–589.
[37] C.J. Perez, A. Vázquez, V.A. Alvarez, Isothermal crystallization of layered silicate/starch-polycaprolactone blend nanocomposites, J. Therm. Anal. Calorim. 91 (2008) 749–757.
[38] J.N. Hay, M. Sabir, L.R.T. Steven, Crystallization kinetics of high polymers. Polyethylene oxide—Part I, Polymer 10 (1969) 187–202.
[39] F.E. Bailey Jr., J.V. Koleske, Poly (Ethylene Oxide), Academic Press, New York, 1976.
[40] D. Turnbull, J.C. Fisher, Rate of nucleation in condensed systems, J. Chem. Phys. 17 (1949) 71–73.
[41] J.D. Hoffman, J.I. Lauritzen Jr., Crystallization of bulk polymers with chain folding: theory of growth of lamellar spherulites, J. Res. Natl. Bur. Stand. 65A (1961) 297–336.
[42] J.I. Lauritzen Jr., J.D. Hoffman, Extension of theory of growth of chain-folded polymer crystals to large undercooling, J. Appl. Phys. 44 (1973) 4340–4352.
[43] S. Vyazovkin, N. Sbirrazzuoli, Isoconversional analysis of calorimetric data on nonisothermal crystallization of a polymer melt, J. Phys. Chem. B 107 (2003) 882–888.
[44] J.D. Hoffman, L.J. Frolen, S.R. Gaylon, J.I. Laurizen Jr., On the growth rate of spherulites and axialites from the melt in polyethylene fractions: regime I and regime II crystallization, J. Res. Natl. Bur. Stand. 79A (1975) 671–699.
[45] J.D. Hoffman, G.T. Davis, J.I. Lauritzen Jr., in: N.B. Hannay (Ed.), Treatise on Solid State Chemistry, vol. 3, Plenum, New York, 1976.
[46] S. Vyazovkin, I. Dranca, Isoconversional analysis of combined melt and glass crystallization data, Macromol. Chem. Phys. 207 (2006) 20–25.
[47] T.W. Chan, A.I. Isaev, Quiescent polymer crystallization: modelling and measurements, Polym. Eng. Sci. 34 (1994) 461–471.
[48] J.D. Hoffman, J.J. Week, Rate of spherulitic crystallization with chain folds in polychlorotrifluoroethylene, J. Chem. Phys. 37 (1962) 1723–1742.
[49] http://athas.prz.rzeszow.pl/.
[50] G.C. Alfonso, T.P. Russell, Kinetics of crystallization in semicrystalline/amorphous polymer mixtures, Macromolecules 19 (1986) 1143–1152.
[51] M. Reading, Modulated differential scanning calorimetry—a new way forward in materials characterization, Trends Polym. Sci. 1 (1993) 248–253.
[52] K. Pielichowski, K. Flejtuch, J. Pielichowski, Step-scan alternating DSC study of melting and crystallisation in poly(ethylene oxide), Polymer 45 (2004) 1235–1242.
[53] B. Wunderlich, Macromolecular Physics, Academic Press, New York, 1980, pp. 27–35.
[54] C. Zhou, S.B. Clough, Multiple melting endotherms of poly(ethylene terephthalate), Polym. Eng. Sci. 28 (1988) 65–68.
[55] I. Okazaki, B. Wunderlich, Reversible melting in polymer crystals detected by temperature-modulated differential scanning calorimetry, Macromolecules 30 (1997) 1758–1764.
[56] B.B. Sauer, W.G. Kampert, E.N. Blanchard, S.A. Threefoot, B.S. Hsiao, Temperature modulated DSC studies of melting and recrystallization in polymers exhibiting multiple endotherms, Polymer 41 (2000) 1099–1108.
[57] F. Cser, F. Rasoul, E. Kosior, Reversible melting of semi-crystalline polymers, J. Therm. Anal. Calorim. 52 (1998) 293–313.